Compressible Fanno flows in micro-channels: an enhanced quasi-2D Fanno-based numerical model

Marco Cavazzuti[1], Mauro A Corticelli[1] and Tassos G Karayiannis[2]

[1] Dipartimento di Ingegneria "Enzo Ferrari", Università degli Studi di Modena e Reggio Emilia, via P. Vivarelli 10, 41125 Modena, Italy

[2] Department of Mechanical and Aerospace Engineering, Brunel University London, Uxbridge, Middlesex UB8 3PH, United Kingdom

Corresponding author e-mail: `marco.cavazzuti@unimore.it`

Abstract. Fanno theory provides an analytical model for the prediction of confined viscous compressible flows under the hypotheses of constant cross-section channel and adiabatic flow. From theory, differentials of flow characteristic quantities can be expressed in function of Mach number and friction factor. Yet, the theory does not assess how to evaluate friction, whereas classical formulas for friction prediction in channels are derived under the hypothesis of incompressible flow and are no longer valid in case of compressible flows. Compressibility deforms the velocity profiles in the channel by making them more flat. As a consequence friction is increased compared to the incompressible case. At the same time, the change in the velocity profiles affects the average dynamic pressure and the bulk temperature along the channel. Correlations, function of Mach and Reynolds numbers, are required for quantifying these changes and improve the prediction of the Fanno model. In the present paper, the impact of compressibility on laminar and turbulent flows in micro-channels is assessed on the basis of a series of CFD simulations, and correlations are presented for friction, average dynamic pressure, and bulk temperature. The correlations are proven to enhance the accuracy of the Fanno model predictions.

1. Introduction

Micro-scale fluid flow is attracting growing interests due to miniaturization in many technological fields. This is primarily true in electronics cooling [1, 2, 3] due to the high dissipated power densities of modern devices. Other applications span a wide range of subjects from refrigeration systems [4] and heat pumps [5] to reactors [6], pipelines [7], and gas bearings [8], to cite a few. Experimental investigations are often difficult and error prone due to the small scale of the problem [9, 10] so that understanding of the fundamental physics is somewhat hampered.

Micro-flows are dominated by surface friction [11] and characterised by large pressure drops. This means compressibility cannot be neglected when the fluid involved is a gas. In early 20th century Fanno and Rayleigh [12] developed theoretical models for the analysis of compressible flow in constant cross-section channels. Their models are based on different assumptions (adiabatic flow for Fanno, isentropic for Rayleigh) and on conservation equations (mass, momentum, and energy) requiring stagnation pressures and temperatures at the channel extremities as boundary conditions for the problem to be solved. Focusing on the Fanno theory (a close parallelism is possible for Rayleigh), flow characteristics such as pressure, temperature, velocity and Mach number, can be predicted at any point along the channel as a function of

Mach number and friction factor once the flow characteristics are known at another location.

This makes it easy to build 1D numerical models solving the flow in the channel iteratively. However, canonical incompressible correlations assuming constant friction in the channel do not hold for compressible flows so that means to predict friction are missing. Considering that boundary conditions are given at stagnation, the dynamic fraction of total pressure and temperature are also required in order to derive the flow characteristics.

The prediction of compressible friction factors has been addressed in the literature by the experimental works of Asako *et al.* [3, 13], and numerically in [14] where correlations are proposed as a function of the Mach number for the case of laminar flow. It is known that compressibility acts by deforming (*i.e.* flattening) the velocity profile along the channel and this necessarily affects both friction and the dynamic pressure and temperature. It is thus necessary to evaluate the entity of the velocity profile deformations to calculate these quantities. Unfortunately, such an evaluation is essentially only possible to be carried out numerically.

In the present work, compressible flow in micro-channels is investigated analysing the velocity profiles extracted at several locations along the channel from a set of CFD results. This allows correlations predicting the compressible friction factor and the average dynamic pressure and temperature values to be found for both laminar and turbulent flow cases, and for both circular and parallel-plate cross-section channels. Correlations are found to be functions of Mach and Reynolds numbers, the latter playing a role only in case of turbulent flow. The correlations are validated and proven to enhance the predictive capability of a 1D micro-channel numerical model based on the Fanno theory that would otherwise lose precision when Mach numbers are incompatible with the incompressible flow assumption. The 1D model, necessarily not including local velocity profiles, by implementing the correlations proposed is able to overcome its intrinsic limitations attaining quasi-2D accuracy.

2. Theoretical background and numerical model

Fanno theory is based on conservation equations (mass, momentum, and energy), ideal gas state equation, and the definitions of Mach number and speed of sound for an ideal gas as in equation (1).

$$\begin{cases} \mathrm{Ma} = U/c = U/\sqrt{\gamma R_\mathrm{g} T} & \text{Mach number} \\ p = \rho R_\mathrm{g} T & \text{Ideal gas state equation} \\ \dot{m} = \rho U A & \text{Mass conservation} \\ c_\mathrm{p} T_0 = c_\mathrm{p} T + U^2/2 & \text{Energy conservation} \\ F_\mathrm{v} = \Delta(p + \rho U^2) A = -\int P f \rho U^2/8 \,\mathrm{d}x & \text{Momentum conservation} \end{cases} \tag{1}$$

Note that in the energy conservation equation stagnation enthalpy $c_\mathrm{p} T_0$ is conserved since the flow is adiabatic, whereas in momentum conservation the resultant of the viscous forces F_v opposes the flow so that the momentum term is not conserved. In equation (1) A is the channel cross-section area, P its perimeter, and f the Darcy friction factor. With a few algebraic changes equation (1) can be written in differential form as

$$\begin{cases} \dfrac{\mathrm{d}p}{p} = \dfrac{-\gamma \mathrm{Ma}^2[1 + (\gamma - 1)\mathrm{Ma}^2]}{2(1 - \mathrm{Ma}^2)} \dfrac{f \,\mathrm{d}x}{D_\mathrm{h}} \\ \dfrac{\mathrm{d}T}{T} = \dfrac{-\gamma(\gamma - 1)\mathrm{Ma}^4}{2(1 - \mathrm{Ma}^2)} \dfrac{f \,\mathrm{d}x}{D_\mathrm{h}} \\ \dfrac{\mathrm{d}U}{U} = -\dfrac{\mathrm{d}\rho}{\rho} = \dfrac{\gamma \mathrm{Ma}^2}{2(1 - \mathrm{Ma}^2)} \dfrac{f \,\mathrm{d}x}{D_\mathrm{h}} \\ \dfrac{\mathrm{dMa}}{\mathrm{Ma}} = \dfrac{\gamma \mathrm{Ma}^2[1 + (\gamma - 1)\mathrm{Ma}^2/2]}{2(1 - \mathrm{Ma}^2)} \dfrac{f \,\mathrm{d}x}{D_\mathrm{h}} \end{cases} \tag{2}$$

where the differentials of the main flow characteristic quantities are expressed as a function of Mach number and friction factor, $D_\mathrm{h} = 4A/P$ being the hydraulic diameter.

With equation (2), once the flow characteristics are known at one location (*e.g.* the entrance section), the channel can be discretized and the flow solved at each node. Flow characteristics at the channel entrance can be predicted iteratively using a shooting technique searching for the inlet conditions that allow the outlet boundary conditions to be met. For a better numerical stability, only the last expression in equation (2) is used for the prediction of Mach number

$$\frac{\mathrm{dMa}}{\mathrm{Ma}} = \frac{\gamma \mathrm{Ma}^2[1 + (\gamma - 1)\mathrm{Ma}^2/2]}{2(1 - \mathrm{Ma}^2)} \frac{f\,\mathrm{d}x}{D_\mathrm{h}} \tag{3}$$

while the other flow characteristics are derived algebraically from equation (1); an inner iterative loop allows the respect of the governing equations with a very strict control over the residuals. An explicit Euler method with a few thousands elements discretization is sufficient for solving any channel with high numerical accuracy and requiring just a few seconds of CPU time on an ordinary PC.

Considering that friction appears explicitly in equation (3), it is important to include in the numerical model correlations for the evaluation of the compressible friction factor. As boundary conditions are better given in terms of total pressure and temperature while the Fanno theory only allows the static quantities to be computed, correlations for evaluating the dynamic fractions of these quantities are also needed for an improved model accuracy. In fact, since velocity profiles are non-uniform, average dynamic pressure and bulk temperature cannot be correctly evaluated from the average quantities available from theory unless suitable correction terms g_p and g_T, larger than unity and function of Mach and Reynolds, are introduced as in equation (4).

$$\begin{cases} p_\mathrm{d,avg} = \dfrac{\int_A \rho U^2/2\,\mathrm{d}A}{\int_A \mathrm{d}A} = g_\mathrm{p} \dfrac{\rho_\mathrm{blk} U_\mathrm{avg}^2}{2} \neq \dfrac{\rho_\mathrm{blk} U_\mathrm{avg}^2}{2} \\ T_\mathrm{d,blk} = \dfrac{\int_A \rho U^3/2c_\mathrm{p}\,\mathrm{d}A}{\int_A \rho U\,\mathrm{d}A} = g_\mathrm{T} \dfrac{U_\mathrm{avg}^2}{2c_\mathrm{p,blk}} \neq \dfrac{U_\mathrm{avg}^2}{2c_\mathrm{p,blk}} \end{cases} \tag{4}$$

The analysis and integration of a large series of velocity profiles from a set of CFD analyses allows these issues to be solved by finding the correlations needed.

3. Simulations setup

A set of more than 90 micro-channel CFD simulations has been solved spanning Reynolds numbers in the laminar and in the turbulent regions ($0 \leq \mathrm{Re} \leq 2 \cdot 10^4$) and Mach numbers in the whole subsonic region ($0 \leq \mathrm{Ma} \leq 1$) for two cross-section types (circular and parallel-plate). The channels have different hydraulic diameters (either $D_\mathrm{h} = 100$ or $500\,\mu\mathrm{m}$), aspect ratios (either $L/D_\mathrm{h} = 100$ or 500), stagnation temperatures (either $T_0 = 300$ or $500\,\mathrm{K}$), and several upstream stagnation pressures p_0. Downstream stagnation pressure p_1 is kept at 1 bar.

Since the flow is highly compressible a stable coupled solver is needed for the simulations. The Ansys Fluent code has been chosen for the purpose. The mesh is either axisymmetric or planar depending on the cross-section type, fully structured, and includes large plenums at the extremities so that boundary conditions are set at locations where static and total quantities almost coincide. The mesh size ranges from 10^5 to $5 \cdot 10^6$ elements, depending on the case examined, in order to grant maximum values of $y^+ \leq 0.3$. An off-scale 500 elements mesh example is given in figure 1. Boundary conditions are total pressure at inlet, static pressure at outlet and no-slip at the wall. Second-order discretization schemes and SST k-ω turbulence

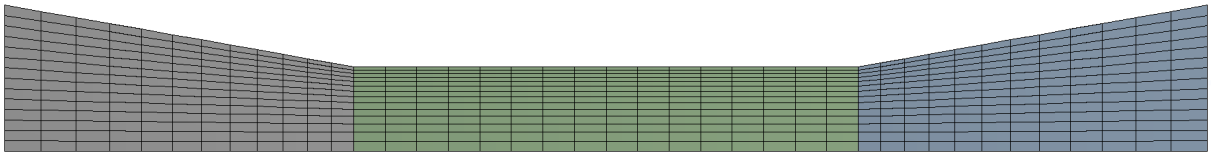

Figure 1. Off-scale mesh example.

model are adopted. The set of equations solved is as follows

$$\begin{cases} \nabla \cdot (\rho \mathbf{U}) = 0 & \text{Mass conservation} \\ \nabla \cdot (\rho \mathbf{U}\mathbf{U}) = -\nabla p + \nabla \cdot \boldsymbol{\tau} & \text{Momentum conservation} \\ \nabla \cdot (\rho \mathbf{U}\,(E + p/\rho)) = \nabla \cdot (\lambda_\mathrm{e} \nabla T + \boldsymbol{\tau} \cdot \mathbf{U}) & \text{Energy conservation} \\ \nabla \cdot (\rho \mathbf{U} k) = \nabla \cdot (\Gamma_\mathrm{k} \nabla k) + G_\mathrm{k} & \text{Transport of } k \\ \nabla \cdot (\rho \mathbf{U} \omega) = \nabla \cdot (\Gamma_\omega \nabla \omega) + G_\omega & \text{Transport of } \omega \end{cases}$$

where $\boldsymbol{\tau}$ is the stress tensor, E the total energy, λ_e the effective thermal conductivity, and $\boldsymbol{\tau} \cdot \mathbf{U}$ the viscous heating term. In the last two expressions Γ is the thermal diffusivity, while the terms G stand for the sum of production, dissipation, and cross-diffusion of the turbulent quantities.

A preliminary mesh convergence study allows the estimation of maximum errors in the prediction of friction $< 0.5\,\%$. During post-processing, average flow characteristics (*e.g.* velocity U, pressure p, temperature T, wall shear stress τ_w) and velocity profiles are extracted at 65 sample locations along the channel for each simulation, summing up to ≈ 6000 sections overall. As the goal of the analysis is to isolate compressibility effects, this set is cleared from samples close to the entrance section where the flow is still far from developed and the entrance effects are relevant: ≈ 3000 samples are left after thisrovide e-mail addresses for any or all of the authors usin operation.

4. Compressibility effects

By plotting the normalized velocity profiles extracted, it is evident that laminar profiles having the same Mach number and turbulent profiles having the same Mach and Reynolds numbers are perfectly superimposable, and their shape changes as shown in figure 2. In particular, both high Mach and high Reynolds numbers make the profiles flatter. This results in larger friction factors, proportional to wall-normal velocity gradients, and smaller correction terms in equation (4). To be noted also that the effect of compressibility depends on the cross-section type, being more evident (*i.e.* resulting in flatter profiles) in the case of circular cross-section.

5. Laminar and turbulent compressible flow correlations

Friction and the dynamic pressure and temperature correction terms in equation (4) can be computed as

$$\begin{cases} f(\mathrm{Ma}, \mathrm{Re}) = \dfrac{8\tau_\mathrm{w}}{\rho_\mathrm{blk} U_\mathrm{avg}^2} \\ g_p(\mathrm{Ma}, \mathrm{Re}) = \dfrac{2p_\mathrm{d,avg}}{\rho_\mathrm{blk} U_\mathrm{avg}^2} \\ g_T(\mathrm{Ma}, \mathrm{Re}) = \dfrac{2c_\mathrm{p,blk} T_\mathrm{d,blk}}{U_\mathrm{avg}^2} \end{cases} \tag{5}$$

where all the terms on the right-hand side are available from the CFD simulations post-processing. These are, the wall shear stress τ_w, the area-weighted average axial velocity U_avg,

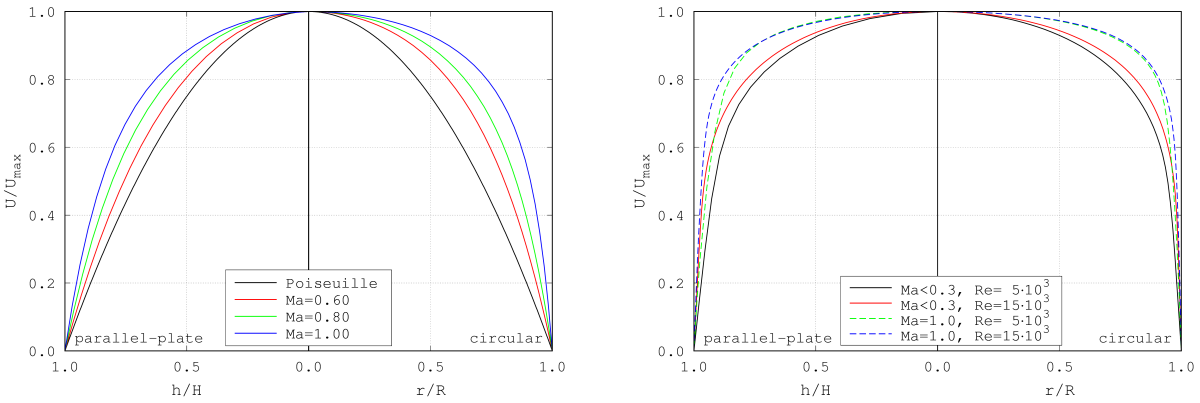

(a) (b)

Figure 2. Normalized velocity profiles for different Mach and Reynolds numbers: (a) laminar case, (b) turbulent case.

and the bulk density ρ_{blk}, specific heat $c_{\text{p,blk}}$ and temperature T_{blk}. This allows plots to be created where these quantities are mapped against Mach and Reynolds numbers. The result of this operation is shown in figure 3. The left-hand side terms in equation (5) only depend on Mach in case of laminar flow. For brevity and better readability, turbulent flow plots are limited to the circular cross-section case and similar plots can be extracted for the parallel-plate cross-section. In figure 3(a) Poiseuille number, defined as $\text{Po} = f\text{Re}$, is plotted on the coordinate axis in place of friction being this quantity more meaningful for the laminar case.

Dots are added to the plots in figure 3 for each of the 3000 sections extracted while lines and surfaces are interpolations of such data. These correspond to the following correlations for the laminar case

$$\text{Po}_{\text{lam}}(\text{Ma}) = \begin{cases} 64\left(1 + 0.653\text{Ma}^2 + 2.809\text{Ma}^3 - 5.311\text{Ma}^4 + 4.157\text{Ma}^5\right) & \text{circular} \\ 96\left(1 + 0.153\text{Ma}^2 + 2.632\text{Ma}^3 - 4.685\text{Ma}^4 + 3.669\text{Ma}^5\right) & \text{parallel-plate} \end{cases} \tag{6}$$

$$g_{\text{p,lam}}(\text{Ma}) = \begin{cases} \dfrac{4}{3} - 0.318\text{Ma}^2 + 0.118\text{Ma}^3 & \text{circular} \\ \dfrac{6}{5} - 0.0530\text{Ma}^2 - 0.0524\text{Ma}^3 & \text{parallel-plate} \end{cases} \tag{7}$$

$$g_{\text{T,lam}}(\text{Ma}) = \begin{cases} 2 - 1.250\text{Ma}^2 + 0.578\text{Ma}^3 & \text{circular} \\ \dfrac{54}{35} - 0.204\text{Ma}^2 - 0.121\text{Ma}^3 & \text{parallel-plate} \end{cases} \tag{8}$$

and for the turbulent case

$$f_{\text{trb}}(\text{Ma}, \text{Re}) = \begin{cases} \left(\dfrac{3.159}{\text{Re}^{0.51-1.57\text{e}-6\text{Re}}}\right)\left(1 + 49.75\dfrac{\text{Ma}^{9.22}}{\text{Re}^{0.47}}\right) & \text{circular} \\ \left(\dfrac{3.744}{\text{Re}^{0.51-1.57\text{e}-6\text{Re}}}\right)\left(1 + 82.58\dfrac{\text{Ma}^{9.24}}{\text{Re}^{0.53}}\right) & \text{parallel-plate} \end{cases} \tag{9}$$

$$g_{\text{p,trb}}(\text{Ma}, \text{Re}) = \begin{cases} 1 + \left(\dfrac{2.789}{\text{Re}^{0.42}}\right)\left(1 - 0.658\dfrac{\text{Ma}^{6.45}}{\text{Re}^{0.103}}\right) & \text{circular} \\ 1 + \left(\dfrac{2.672}{\text{Re}^{0.44}}\right)\left(1 - 0.276\dfrac{\text{Ma}^{8.91}}{\text{Re}^{0.028}}\right) & \text{parallel-plate} \end{cases} \tag{10}$$

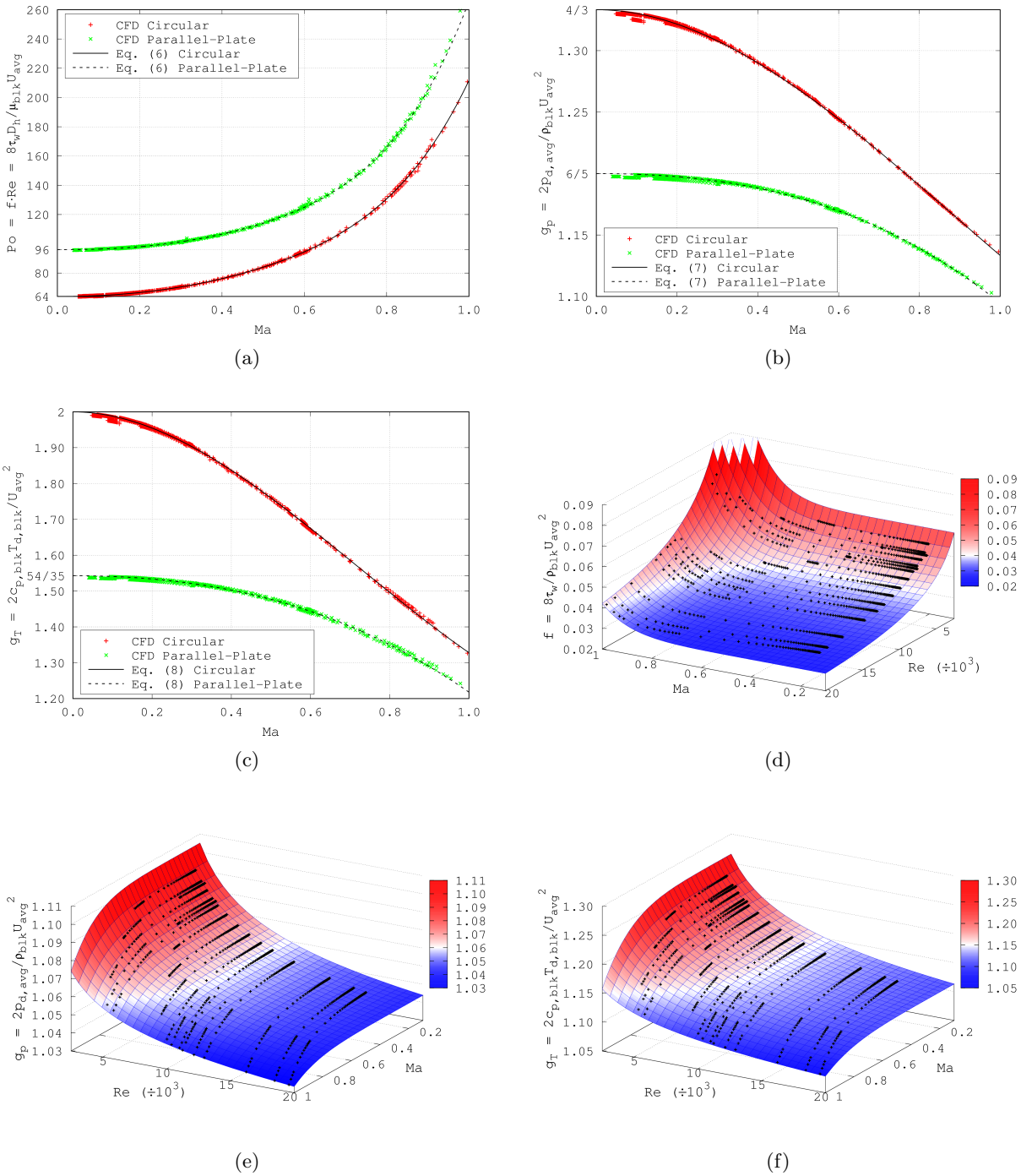

Figure 3. Compressible friction factor and correction terms (dots) extracted from CFD analyses as function of Mach and Reynolds numbers, and their interpolations (lines and surfaces): (a) Po(Ma) laminar case, (b) g_p(Ma) laminar case, (c) g_T(Ma) laminar case, (d) f(Ma, Re) circular-cross section turbulent case, (e) g_p(Ma, Re) circular-cross section turbulent case, (f) g_T(Ma, Re) circular-cross section turbulent case.

$$g_{\mathrm{T,trb}}(\mathrm{Ma},\mathrm{Re}) = \begin{cases} 1 + \left(\dfrac{6.603}{\mathrm{Re}^{0.41}}\right)\left(1 - 1.230\dfrac{\mathrm{Ma}^{5.53}}{\mathrm{Re}^{0.141}}\right) & \text{circular} \\ 1 + \left(\dfrac{5.591}{\mathrm{Re}^{0.42}}\right)\left(1 - 2.188\dfrac{\mathrm{Ma}^{7.84}}{\mathrm{Re}^{0.223}}\right) & \text{parallel-plate} \end{cases} \tag{11}$$

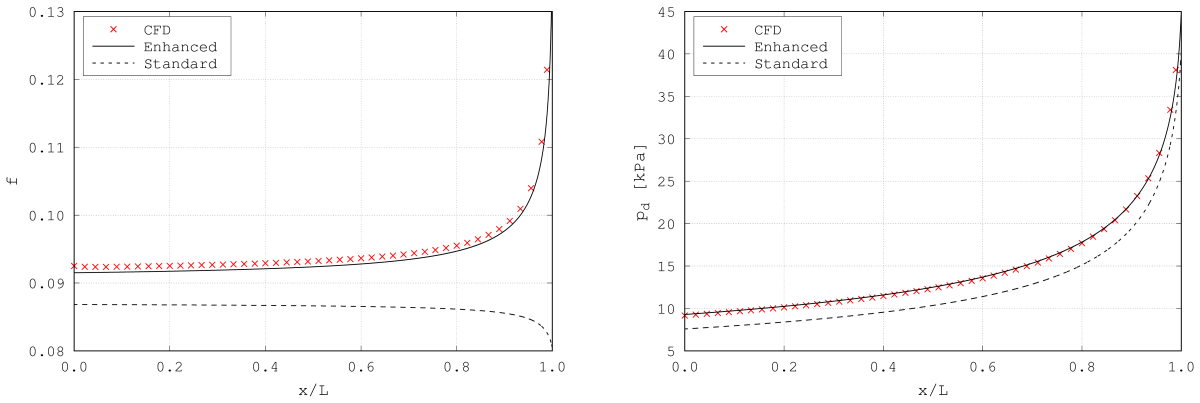

(a) (b)

Figure 4. Model validation: CFD *vs* enhanced and standard 1D Fanno flow model: (a) friction factor, (b) dynamic pressure along the channel.

Note that compressibility effects quickly fade away for Mach numbers close to zero while they grow very strong as Mach approaches unity. In the limit, laminar incompressible results shown in low Mach areas of figures 5(a)-(c) are in line with Poiseuille theory. For the same reason, turbulent correlations in equations (9)-(11) are composed of two terms: one modelling the incompressible behaviour at low Mach where only Reynolds appears, the other modelling the compressible flow in function of both Mach and Reynolds numbers. The incompressible term used in equation (9) for friction gradually tends to Blasius correlation for growing Reynolds. The average interpolation error of the given correlations is $< 0.5\,\%$ for the laminar case, and $< 2.0\,\%$ for the turbulent case.

6. Validation

The enhanced Fanno-based 1D model implementing the correlations in equations (6)-(11) is compared to the standard model where friction is computed following incompressible flow theory, and where dynamic pressure and temperature correction terms are set to unity. The benchmark is given by additional CFD simulations performed under different operating conditions. As an example, figure 4 shows the evolution on friction factor and dynamic pressure along the channel for the case of circular cross-section with $D_\mathrm{h} = 40\,\mu\mathrm{m}$, $L/D_\mathrm{h} = 450$, $T_0 = 300\,\mathrm{K}$, $p_0 = 7.0\,\mathrm{bar}$, and $p_1 = 0.5\,\mathrm{bar}$. Under these circumstances the flow is laminar and choked.

As shown, the enhanced model approximates much better the laminar CFD results. Similar results can be drawn for the turbulent case. In particular, in case of fully turbulent flow, the dynamic pressure and temperature correction terms lose significance since they progressively tend to unity for growing Reynolds. On the contrary, in case of moderately turbulent flows, where the gradients in figure 3(d) are still large, the error in friction prediction using the standard model can be as large as $50\,\%$ and more.

7. Conclusions

An enhanced 1D model for solving compressible Fanno flow in circular and parallel-plate cross-section channels under both laminar and turbulent flow conditions is presented.

The model implements a set of correlations, calibrated on the basis of a series of CFD simulations, for the assessment of friction factor, dynamic pressure, and dynamic temperature at each section addressing the effects of compressibility. Correlations are derived from a detailed analysis of the velocity profiles and their change in shape at different Mach and Reynolds

numbers. This gives the model 2D accuracy, overcoming the instrinsic limits of a 1D approach.

The model has been successfully validated over additional simulations in which the predictive capability of the enhanced model has been shown to be significantly improved over that of a standard model not implementing the proposed correlations. As such, the enhanced model provides a fast and accurate tool for solving confined compressible flows that can be used in the design of real-life micro-channel applications.

Due to the similarities among Fanno and Rayleigh theories, an extension of the model in order to include heat transfer should not be difficult from the numerical point of view.

References

[1] Kohl M J, Abdel-Khalik S I, Jeter S M and Sadowski D L 2005 An experimental investigation of microchannel flow with internal pressure measurements *Int. J. Heat Mass Tran.* **48(8)** 1518–33
[2] Hong C, Nakamura T, Asako Y and Ueno I 2016 Semi-local friction factor of turbulent gas flow through rectangular microchannels *Int. J. Heat Mass Tran.* **98** 643–9
[3] Kawashima D and Asako Y 2014 Data reduction of friction factor of compressible flow in micro-channels *Int. J. Heat Mass Tran.* **77** 257–61
[4] Deodhar S D, Kothadia H B, Iyer K N and Prabhu S V 2015 Experimental and numerical studies of choked flow through adiabatic and diabatic capillary tubes *Appl. Therm. Eng.* **90** 879–94
[5] Agrawal N and Bhattacharyya S 2007 Adiabatic capillary tube flow of carbon dioxide in a transcritical heat pump cycle *Int. J. Energ. Res.* **31** 1016–30
[6] Mignot G P, Anderson M H and Corradini M L 2009 Measurement of supercritical CO2 critical flow: effects of L/D and surface roughness *Nucl. Eng. Des.* **239(5)** 949–55
[7] Kostowski W J and Skorek J 2012 Real gas flow simulation in damaged distribution pipelines *Energy* **45** 481–8
[8] Plante J-S, Vogan J, El-Aguizy T and Slocum A H 2005 A design model for circular porous air bearings using the 1D generalized flow method *Precis. Eng.* **29(3)** 336–46
[9] Morini G L 2018 The challenge to measure single-phase convective heat transfer coefficients in microchannels *Heat Transfer Eng.* (In press)
[10] Rosa P, Karayiannis T G and Collins M W 2009 Single-phase heat transfer in micro-channels: the importance of scaling effects *Appl. Therm. Eng.* **29** 3447–68
[11] Cioncolini A, Scenini F, Duff J, Szolcek M and Curioni M 2016 Choked cavitation in micro-orifices: an experimental study *Exp. Therm. Fluid Sci.* **74** 49–57
[12] Strutt J W 1910 Aerial plane waves of finite amplitudes *Proc. Roy. Soc. Lond.* A **84(570)** 247–84
[13] Asako Y, Pi T, Turner S E and Faghri M 2003 Effect of compressibility on gaseous flows in micro-channels *Int. J. Heat Mass Tran.* **46(16)** 3041–50
[14] Cavazzuti M, Corticelli M A and Karayiannis T G 2019 Compressible Fanno flows in micro-channels: an enhanced quasi-2D numerical model for laminar flows *Therm. Sci. Eng. Progr.* **10** 10–26